Journal Name

ARTICLE

High-detectivity Ultraviolet Photodetectors based on Laterally Mesoporous GaN

Received 00th January 20xx,
Accepted 00th January 20xx

DOI: 10.1039/x0xx00000x

www.rsc.org/

Lei Liu[a, b], Chao Yang[a, b], Amalia Patanè[c], Zhiguo Yu[a], Faguang Yan[b, d], Kaiyou Wang[b, d], Hongxi Lu[a], Jinmin Li[a, b] and Lixia Zhao*[a, b]

Photodetectors for the ultraviolet (UV) range of the electromagnetic spectrum are in great demand for several technologies, but require the development of novel device structures and materials. Here we report on the high detectivity of UV photodetectors based on well-ordered laterally mesoporous GaN. The specific detectivity of our devices under UV-illumination reaches values of up to 5.3×10^{14} Jones. We attribute this high specific detectivity to the properties of the mesoporous GaN/metal contact interface: the trapping of photo-generated holes at the interface lowers the Schottky barrier height thus causing a large internal gain. The high detectivity along with the simple fabrication process make these laterally mesoporous GaN photodetectors of great potential for applications that require selective detection of weak optical signals in the UV range.

Introduction

Since the first report of mesoporous silica in 1990s,[1] porous materials, in particular mesoporous materials, have been extensively investigated and widely used in various applications, such as energy conversion and storage,[2-4] water splitting,[5-7] heteroepitaxial growth[8, 9] and distributed Bragg reflectors (DBRs).[10, 11] In general, mesoporous materials have pores with size between 2 and 50 nm,[12] and can have exceptional properties including a large surface-to-volume ratio, and tunable bandgap energy and refractive index.[13, 14] In addition, nanoscale effects in their mesochannels and on their pore walls act to reduce the interface migration distance.[15] The reduced interface migration distance as well as the large surface-to-volume ratio can decrease the carrier migration time and also increase the photo-carrier lifetime, which are both desirable in light detection and harvesting. Till now, various photodetectors and solar cells based on mesoporous semiconductors have been reported including mesoporous Silicon, perovskite and Gallium Nitride (GaN).[16-18] Among these semiconductors, GaN represents an ideal candidate not only for light emitting diodes (LEDs)[19, 20], but also for visible blind UV detectors that are needed in various applications, such as flame detection, environmental monitoring and UV astronomy.[21] Compared with the Silicon-based counterpart, GaN-based UV photodetectors offer many advantages, such as a wide direct bandgap, a high electron saturation drift velocity, an intrinsic ultraviolet absorption window, chemical and thermal stability, *etc*.[22, 23] However, the performance of the currently available GaN-based UV detectors is not yet adequate for applications that require the detection of weak optical signals. Different methods have been used to improve their performance, including avalanche photodetection and coupling of light to surface plasmons.[24-28] Mesoporous GaN may offer an alternative approach, which is still largely unexplored.

Although there have been reports on mesoporous GaN-based photodetectors, previous works have focused mainly on vertical or 3D mesoporous GaN.[29-32] Recently, a new type of mesoporous GaN, laterally mesoporous GaN, has generated increasing interest because of its many advantages compared to vertical and 3D mesoporous GaN: (*a*) it is better suited for device fabrication due to its flat surface; (*b*) it could be used to fabricate large scale (> 500 μm) mesoporous templates along the direction of the mesopores; (*c*) it is birefringent and exhibits favourable electronic transport properties.[10, 33] Due to these advantages, laterally mesoporous GaN has been used in optoelectronic applications.[34, 35] However, it has not yet been exploited for light detection.

Here we report on the fabrication of well-ordered laterally mesoporous GaN and its implementation in metal-semiconductor-metal (MSM) photodetectors with specific detectivity D^* up to 5.3×10^{14} Jones under UV illumination (λ = 340 nm). This is by far the highest ever reported for GaN-based UV photodetectors.[36-38] Our findings and analysis indicate that this new type of device structure has potential for applications that require selective detection of weak UV light.

[a] *Semiconductor Lighting Research and Development Center, Institute of Semiconductors, Chinese Academy of Sciences, A35 Qinghua East Road, Haidian District, Beijing, 100083, P. R. China.*
[b] *College of Materials Science and Opto-Electronic Technology, University of Chinese Academy of Sciences, No.19A Yuquan Road, Beijing, 100049, P. R. China.*
[c] *School of Physics and Astronomy, The University of Nottingham, Nottingham NG7 2RD, United Kingdom.*
[d] *SKLSM, Institute of Semiconductors, CAS, P. O. Box 912, Beijing, 100083, P. R. China.*
* E-mail: lxzhao@semi.ac.cn.
Electronic Supplementary Information (ESI) available: [details of any supplementary information available should be included here]. See DOI: 10.1039/x0xx00000x

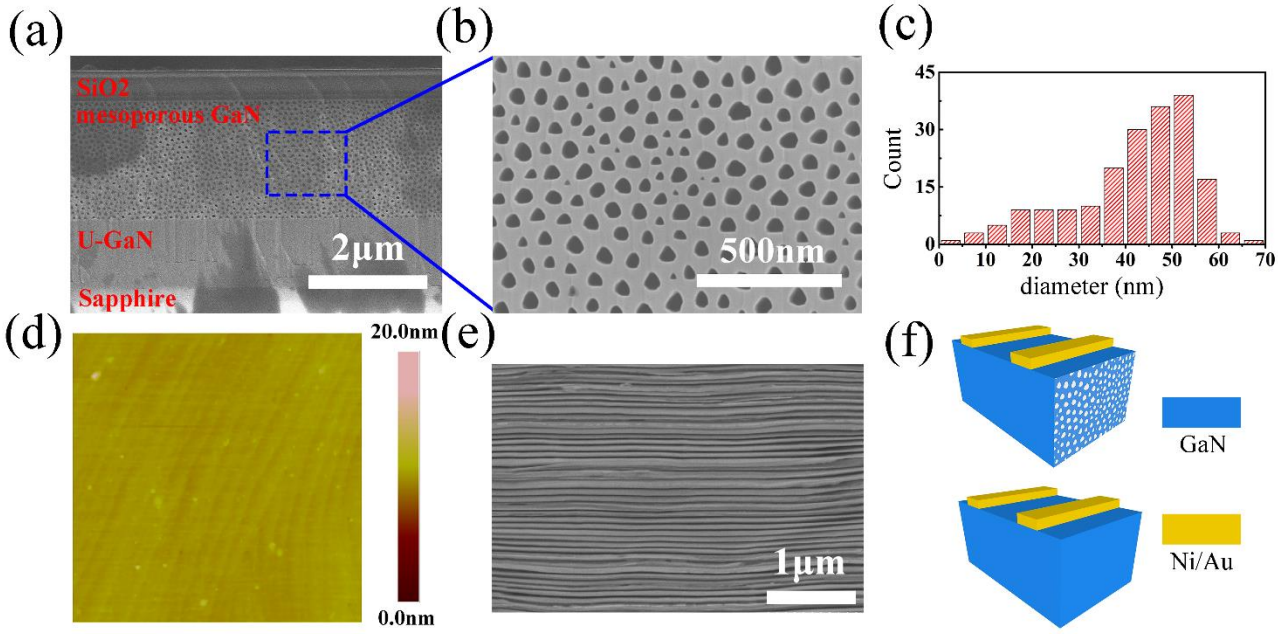

Fig. 1 (a) SEM cross-section image of the mesoporous GaN and the magnified image of the mesopores (b); (c) the size distribution of the mesopores; (d) AFM image of the top GaN surface after the electro-chemical etching; (e) SEM image of the mesoporous GaN after the removal of the surface GaN layer; (f) schematic diagram of the mesoporous (PD_A) and non-mesoporous (PD_B) GaN photodetector.

Experimental results and discussions

We used an electro-chemical etching process to transform a ~2-μm-thick n^+-GaN layer into laterally mesoporous GaN. The n^+-doping of GaN is needed due to the selective etching of electrical conductive GaN.[10] Fig. 1(a) and (b) show the scanning electron microscopy (SEM) cross-section images of our laterally mesoporous n^+-GaN. The shape of the mesopores varies from triangle-like to circle-like, indicating that both anisotropic etching and isotropic etching occur during the conversion of n^+-GaN into mesoporous GaN[39]. Statistical analysis of the mesopores shows that their size ranges from ~ 3 to 70 nm with average size of ~ 42 nm (Fig. 1(c)). In addition, we estimate the surface-to-volume ratio, porosity and the specific surface area to be 3.04×10^4 m^{-1}, 25% and ~ 500 m^2g^{-1}, respectively. Our atomic force microscopy (AFM) studies (Fig. 1d) indicate that following the electro-chemical etching, the GaN top surface remains almost flat on the atomic scale with an average surface roughness of about 0.15 nm (as determined by the standard deviation of the surface height distribution). To reveal the morphology of the mesopores along their elongated direction, a thin mesoporous GaN surface layer was exposed using reactive ion etching induced coupled plasma. As shown in Fig. 1(e), the mesopores are well-ordered along the direction of electro-chemical etching [See Fig. S1 in the Supporting Information].

Metal-semiconductor-metal (MSM) photodetectors were fabricated using the mesoporous GaN. Photodetectors based on non-mesoporous n^+-GaN were also fabricated and used as reference samples. The photodetectors with mesoporous and non-mesoporous GaN, labelled PD_A and PD_B, respectively, are schematically illustrated in Fig. 1(f).

Fig. 2(a) shows the current density versus applied voltage (*J-V*) curves under dark and UV light illumination (λ = 340 nm, I_{light} = 1.68 $mWcm^{-2}$) for PD_A (mesoporous) and PD_B (non-mesoporous). The dark current density, J_{dark}, for PD_A is ~ 0.06 Acm^{-2} at V = 1V and is considerably smaller than for PD_B (J_{dark} ~ 0.6 Acm^{-2}). The lower dark current density in PD_A is attributed to the reduction of the background carrier density following the conversion of n^+-GaN into a mesoporous structure.[10] Under UV light illumination, the current density for PD_B is almost identical to the dark value and no measurable photo-response is observed. However, for PD_A, there is a strong photo-response with a current density J_{light} ~17 Acm^{-2} at V = 1V. Thus the conversion of bulk n^+-GaN into mesoporous GaN leads to a significant improvement in the photo-sensitivity to UV light illumination.

To evaluate the spectral response of the mesoporous GaN photodetector (PD_A), the photocurrent spectra was measured in the range λ = 300–400 nm at V = 1V and 0.5V. As shown in Fig. 2(b), the photodetector is very sensitive to photons with wavelength λ < 350 nm. In contrast, for λ > 350 nm the sensitivity decreases and illumination with photons of wavelength larger than λ ~ 380 nm induces a much weaker photoresponse. The UV/visible rejection ratio, which we define as the ratio between the photoresponse at λ = 350 nm and λ = 400 nm, is ~100 and ~400 at V = 1V and V = 0.5V, respectively. These large rejection ratios demonstrates selective detection of the photodetector to UV light.

To further evaluate the performance of PD_A, we examined the specific detectivity, D^*, and responsivity, R, at λ = 340 nm. The specific detectivity is a figure of merit of a detector that

describes the smallest detectable optical signal and can be expressed as[40, 41]

$$D^* = \frac{R}{(2eJ_{dark})^{\frac{1}{2}}}, \quad (1)$$

increase of the dark current density dominates over the increase of R, leading to the saturation and decrease of D^* at high V.

From equation (2) for R and the measured values of R, we

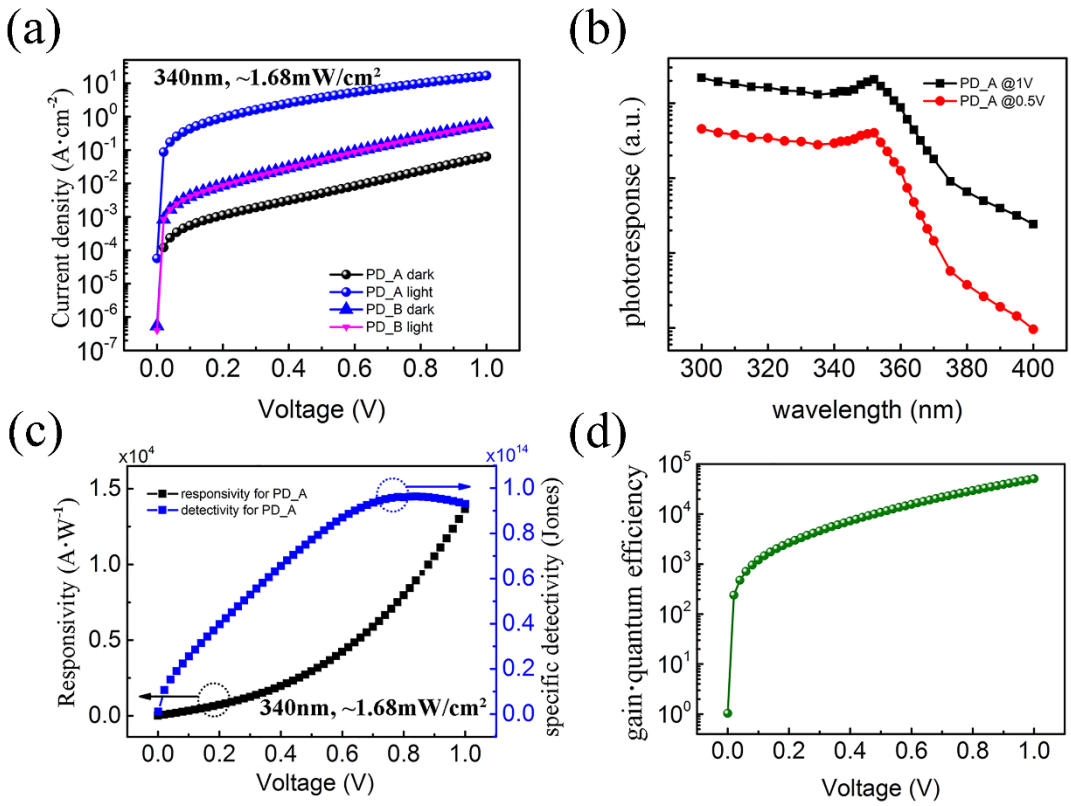

Fig. 2 (a) Current density versus the applied voltage under dark and under UV light illumination (340 nm, ~1.68 mWcm^{-2}) for PD_A (mesoporous) and PD_B (non-mesoporous); (b) spectral selectivity of PD_A (mesoporous) at 1V and 0.5V bias; (c) responsivity and specific detectivity of the mesoporous GaN photodetector (PD_A) versus the applied voltage; (d) product of the gain and quantum efficiency versus the applied voltage for the mesoporous GaN photodetector (PD_A).

where e is the electron charge. The responsivity R can be expressed as

$$R = \frac{J_{Ph}}{I_{light}} = \frac{J_{light} - J_{dark}}{I_{light}} = g\eta\frac{e}{hc/\lambda}, \quad (2)$$

where J_{ph} is the photocurrent density (*i.e.* $J_{ph} = J_{light} - J_{dark}$), I_{light} is the incident light power intensity, g is the internal gain, η is the quantum efficiency, and h, c and λ are the Planck's constant, speed of light and the wavelength of incident light, respectively.

Fig. 2(c) shows the bias dependence of the responsivity R and specific detectivity D^* for PD_A in the range V = 0 to 1V at λ = 340 nm (I_{light} = 1.68 mWcm^{-2}). The responsivity (black curve) increases monotonically with increasing V, reaching values as high as R ~10^4 AW^{-1} at V = 1V. In contrast, the specific detectivity (blue curve) increases with increasing V, but reaches a plateau at V = 0.7V followed by a decrease for V > 0.9 V. The maximum value of D^* is about 1.0×10^{14} cmHz$^{1/2}$W^{-1} (Jones) at V = 0.8V. The bias dependence of the specific detectivity D^* can be explained by examining the expression for D^* from equation (1). With increasing V, both the responsivity (Fig. 2c) and the dark current density (Fig. 2a) increase. For V < 0.8V, the responsivity increases with V more strongly than the dark current density, leading to an increase of D^*. In contrast, for V > 0.8V the estimate the product of the internal gain g and quantum efficiency η. As shown in Fig. 2(d), the product $g\eta$ increases with increasing applied voltage and reaches a value of ~5×10^4 at V = 1V. Since η < 100%, we deduce a large internal gain g > 5×10^4. An internal gain was reported before for MSM photodetectors and is desirable for applications requiring high responsivity.[42-44] Several mechanisms can explain an internal gain, including photoconductive gain,[45] avalanche carrier multiplication at high electric fields,[24] and trapping of photo-generated carriers (mainly holes) at the semiconductor/metal interface.[46] For our mesoporous GaN photodetector, we propose that the trapping of photo-generated carriers at the GaN/metal interface is the

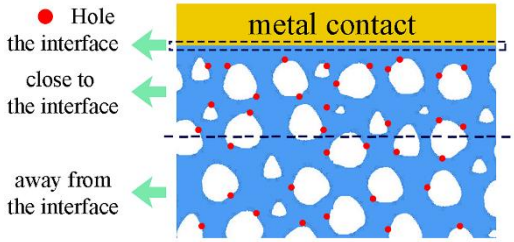

Fig. 3 Schematic of the surface states close to and away from the interface of mesoporous GaN/metal contact.

dominant mechanism. The photo-generated carriers act to decrease the height of the Schottky barrier at the semiconductor/metal interface, thus increasing the photocurrent. In particular, the gain could be significantly enhanced in mesoporous GaN due to the large surface-to-volume ratio and corresponding large density of trapping centers at the GaN/metal interface. As shown schematically in Fig. 3, surface states in mesoporous GaN occur in the whole structure. However, only those close to the interface can affect the height of the Schottky barrier and hence the gain.[47]

Since surface states can be effectively reduced using a passivation layer,[48, 49] we fabricated a mesoporous GaN photodetector with a 5-nm-thick HfO_2 passivation layer on the top surface of the mesoporous GaN (sample PD_C) and compared it with PD_A. Fig. 4(a) and 4(b) show the photocurrent and the specific detectivity D^* of PD_A and PD_C, respectively, for incident UV (λ = 340 nm) light of power P. It can be seen that D^* decreases with increasing power for both devices. The larger values of D^* are obtained in PD_A. The maximum specific detectivity for PD_A is $D^* = 5.3\times10^{14}$ Jones at $P \sim 0.11$ μW, which is so far the highest reported specific detectivity for GaN-based UV photodetectors.[36-38]

We note that the photocurrent increases non-linearly with increasing P. The non-linear relationship can be described well by a simple power law, *i.e.* $I \propto P^{\vartheta}$, where ϑ ($0 < \vartheta \leq 1$) is a parameter related to the trapping of the photo-generated carriers, with larger ϑ corresponding to a weaker trapping.[50-52] From the fits to the data in Fig. 4(a) and 4(b), we find ϑ = 0.20 and 0.66 for PD_A and PD_C, respectively, indicating less significant trapping in PD_C. This observation is in line with the model of photo-generated carrier trapping at the mesoporous GaN/metal interface as the trapping of carriers by surface states can be reduced by the HfO_2 passivation layer.

The trapping of the photo-generated carriers can also be seen in the time-resolved measurements. The time-resolved photocurrent of PD_A and PD_C was measured by the temporal modulation of a UV-LED via a signal generator and a power amplifier [also see supplementary Fig. S2]. As shown in Fig. 4(c) and 4(d), the yellow and pale blue regions correspond to cycles during which the UV-LED is on and off, respectively. The rise and decay times of the photocurrent are larger than 20s and 60s, respectively, for PD_A. These times are one to two orders magnitude longer than those for PD_C. The longer rise and decay times for PD_A are attributed to the trapping and de-trapping (emitting) of photo-generated carriers and support the trapping model for the mesoporous GaN/metal interface.

To explain the gain, we consider the schematic energy band diagram in Figure 5. As shown in Fig. 5(a), without illumination,

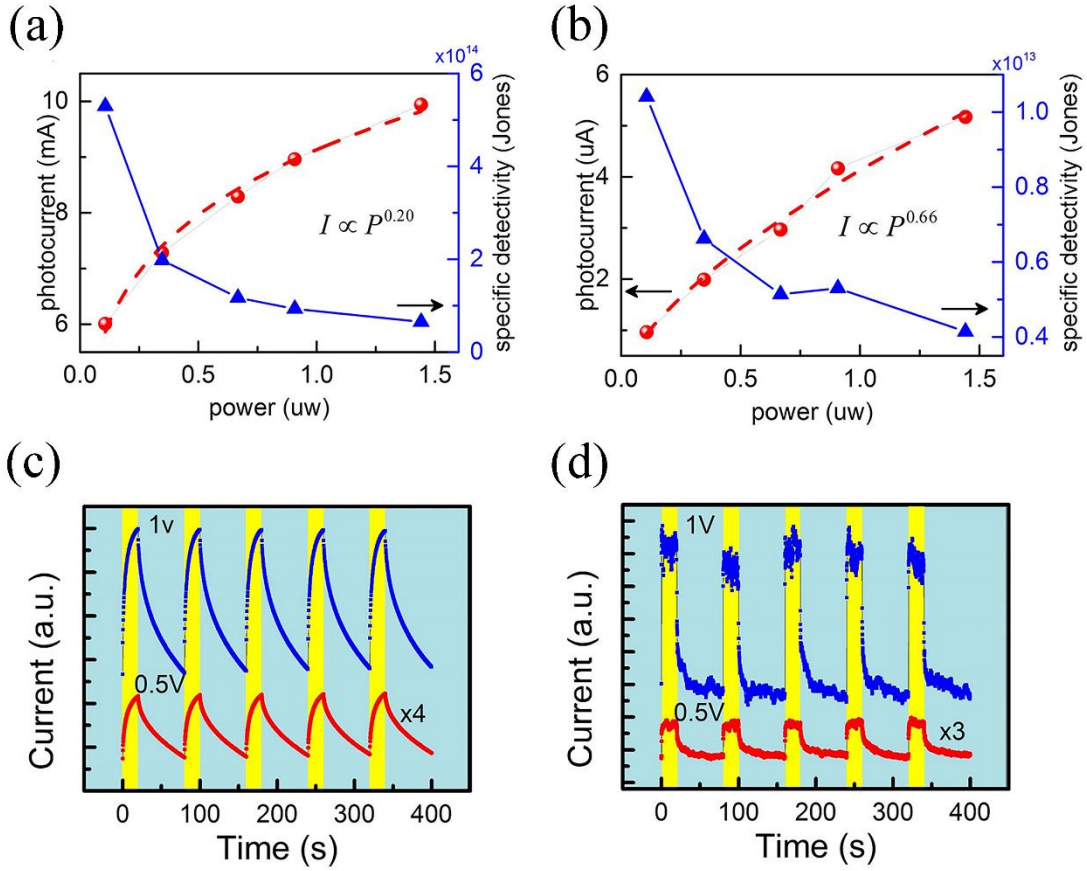

Fig. 4 (a) (b) Power-dependence of the photocurrent and specific detectivity for the mesoporous GaN photodetector (PD_A) and mesoporous GaN photodetector with HfO_2 passivation layer (PD_C); (c) (d) time-dependence of the current for the mesoporous GaN photodetector (PD_A) and mesoporous GaN photodetector with HfO2 passivation layer (PD_C).

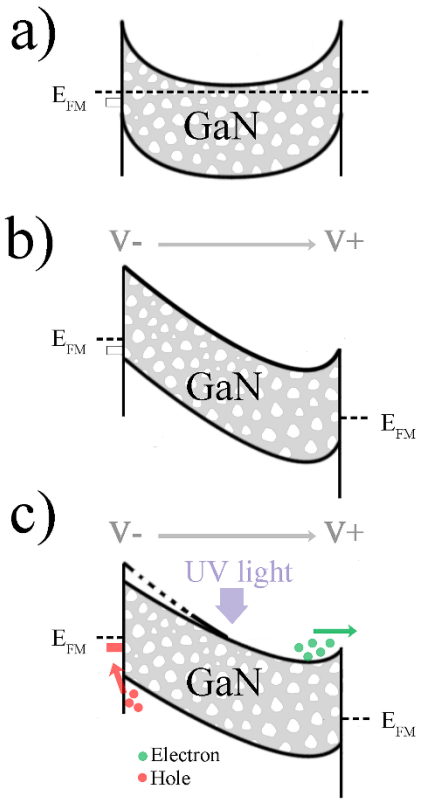

Fig. 5 Schematic energy band diagrams of a mesoporous photodetector under (a) zero bias and without UV illumination, (b) applied bias, and (c) applied bias and light illumination.

the band bending at the interface of mesoporous GaN and the metal contacts forms two back-to-back Schottky junctions. At the mesoporous GaN/metal interface, ionized acceptor-like surface states (trapping centers) exist below the Fermi level (illustrated using a black box). Under an applied bias, a depletion region forms, as shown in Fig. 5(b). Under light illumination, light generates electron-hole pairs; the electrons and holes photo-generated in the depletion region are separated by the applied bias and drift to the positively and negatively biased contacts, respectively. The photo-generated holes drift to the negatively biased contact and are captured by the trapping centers at the mesoporous GaN/metal interface, thus producing a net positive charge. In turns, this acts to lower the height of the Schottky barrier at the negatively biased contact compared to the case of no illumination.[42, 44, 46, 53] The lowered Schottky barrier under UV light illumination increases the thermionic current, resulting in a large photocurrent and internal gain.

The height of the Schottky barrier can be calculated from the Schottky thermionic current:

$$I = I_1\left(\exp\left(\frac{eV}{nK_BT}\right) - 1\right) + I_2\left(\exp\left(-\frac{eV}{nK_BT}\right) - 1\right), \quad (3)$$

$$I_1 = AA^*T^2\exp(-e\varphi_{b1}/K_BT), \quad (4)$$

$$I_2 = AA^*T^2\exp(-e\varphi_{b2}/K_BT), \quad (5)$$

where A is the area of the photodetector, A^* is the effective Richardson constant, e is the electron charge, V is the applied voltage, n is the ideality factor, T is absolute temperature, K_B is the Boltzmann constant and $q_{\varphi b1}$ and $q_{\varphi b2}$ are the heights of the Schottky barriers at the two contacts. By fitting the measured *J-V* curves in Fig. 3(a) with the equations above, we obtain $q_{\varphi b1} = q_{\varphi b2}$ =0.58 eV for the PD_A in the dark, and $q_{\varphi b1} = q_{\varphi b2}$ =0.37 eV under UV light illumination (λ = 340 nm, ~1.68 mWcm^{-2}). Thus, the height of the Schottky barrier is significantly decreased by UV light, resulting in a larger photocurrent.

Our schematic energy band diagram is consistent with the time-resolved measurement results. When light is switched on, the trapping centers capture the photo-generated holes, decreasing the height of the Schottky barrier and increasing the photocurrent. Because the capture rate is proportional to the density of empty traps, the capture rate gradually decreases as the traps are occupied by the photo-generated holes. Thus the Schottky barrier height gradually decreases with time and the photocurrent increases until it reaches a plateau, consistent with our time-resolved response measurements. However, when the light is switched off, the holes can escape from the traps. Thus the Schottky barrier tends to recover its height and the photocurrent gradually decreases. The photodetector behaves like a capacitor. The lowering and recovery sequences for the Schottky barrier can be compared to the charge and discharge of a capacitor, respectively. We have carried out a series of time-resolved measurements with different light switching periods ranging from 500 μs to 100 ms [see Fig. S2 in the Supporting Information]. Although the photo-response decreases with increasing switching frequency, f, a large photocurrent（100 μA) is still obtained at f =2× 10^3 Hz. Thus laterally mesoporous GaN photodetectors could be used for fast detection of weak UV signals.

Conclusion

In summary, we have fabricated metal-semiconductor-metal photodetectors based on well-ordered laterally mesoporous GaN. The conversion of GaN into a mesoporous structure leads to a significant performance improvement. The specific detectivity of our devices under UV illumination (340 nm) can reach values of up to 5.3×10^{14} Jones at applied voltages of 1V. We attribute this high detectivity to the large internal gain caused by the trapping of photo-generated holes at the interface between the mesoporous GaN and the metal contact. This charge trapping reduces the height of the Schottky barrier at the mesoporous GaN/metal contact interface, thus increasing the thermionic current. The high-detectivity along with the simple fabrication process make these laterally mesoporous photodetectors useful for the selective detection of weak optical signals in the UV spectral range.

Experimental Section

Epilayers: The investigated GaN epilayers were grown on (0001) sapphire substrate using metal-organic chemical vapor deposition. Firstly, the sapphire was thermally cleaned under H_2 at 1100℃ for 10 minutes. After that, a ~30-nm-thick low

temperature GaN buffer layer was grown onto the sapphire substrate at 525℃. Subsequently, a ~1-μm-thick undoped GaN layer was grown at 1060℃, followed by a ~2-μm-thick n^+-GaN:Si layer (3×10^{18}cm^{-3}) grown at 1045℃.

Etching process and mechanism: The ~2-μm-thick *n*-type bulk GaN layer was transformed into laterally mesoporous GaN using an electro-chemical etching process. As shown schematically in Fig. S1 (a), before etching, a ~800-nm-thick SiO_2 protective layer was deposited onto the GaN epilayer to avoid the etching of the top GaN surface. Subsequently, a laser-scribing process was performed to form the lateral etching channels (windows) with a 550 μm spacing. During the etching, n^+-GaN contacted with platinum metal was used as anode, and a platinum contact was used as cathode. The etching mechanism is depicted in Fig. S1 (b). With the n^+-GaN immersed in the nitric acid (65 wt%) electrolyte, a Schottky junction is formed at the GaN/electrolyte interface. Under an external applied DC voltage, the n^+-GaN is oxidized by holes near the GaN/electrolyte interface:[15]

$$GaN + 3H_2O + 3h^+ = Ga(OH)_3 + \frac{1}{2}N_2 + 3H^+. \quad (6)$$

Since the oxidized product of GaN ($Ga(OH)_3$) is not thermodynamically stable in the acid electrolyte, it dissolves into Ga^{3+}:

$$Ga(OH)_3 + 3H^+ = Ga^{3+} + 3H_2O\ . \quad (7)$$

Then the mesopores form where the GaN dissolves. After etching, the SiO_2 protective layer was removed using diluent HF, and the wafers were ultrasonically cleaned in DI water and dried in N_2.

Device fabrication: Semi-transparent interdigitated Schottky contacts made of a Ni (5 nm)/ Au (5 nm) multilayer were deposited using e-beam evaporation. The pattern was defined by standard lithography and lift-off techniques. Thereafter, a Ti (50 nm)/ Au (300 nm) multilayer was patterned and evaporated to form the contact pads. The fingers are 10-μm-wide and 200-μm-long with 5-μm-wide inter-finger spacing. The active area of the photodetectors is 260×200 μm^2. The 5-nm-thick HfO_2 layer was deposited via atomic layer deposition using $Hf(NMe_2)_4$ and water with nitrogen as carrier gas. The pressure and temperature are 0.2 Torr and 120℃, respectively. The thickness per growth cycle is ~0.13nm/cycle and the total growth cycles are 38.

Measurement setup: The photo and dark current density–voltage (*J-V*) characteristics of the photodetectors were measured using an Agilent semiconductor parameter analyzer B1500A, and the light output from a 150W Xe lamb was directed into a monochromator for single wavelength selection. The incident optical power onto the photodetectors was measured using a calibrated power meter (Thorlabs GmbH., PM 100D). The power-dependent response was measured using an attenuator to change the incident light power. The time-resolved response was measured using a UV-LED, a signal generator and a power amplifier.

Acknowledgements

This work was supported by the National Natural Science Foundation of China (11574306), the National Basic Research and High Technology Program of China (2015AA03A101, 2014CB643903, 2014BAK02B08 and 2015AA033303).

References

1 D. Y. Zhao, J. L. Feng, Q. S. Huo, N. Melosh, G. H. Fredrickson, B. F. Chmelka and G. D. Stucky, *Science*, 1998, **279**, 548-552.
2 W. Li, J. Liu and D. Zhao, *Nature Reviews Materials*, 2016, **1**, 16023.
3 Z. S. Wu, Y. Sun, Y. Z. Tan, S. B. Yang, X. L. Feng and K. Mullen, *J Am Chem Soc*, 2012, **134**, 19532-19535.
4 U. Bach, D. Lupo, P. Comte, J. E. Moser, F. Weissortel, J. Salbeck, H. Spreitzer and M. Gratzel, *Nature*, 1998, **395**, 583-585.
5 H. Tüysüz and C. K. Chan, *Nano Energy*, 2013, **2**, 116-123.
6 S. Chen and S. Z. Qiao, *Acs Nano*, 2013, **7**, 10190-10196.
7 Y. Hou, Z. Wen, S. Cui, S. Ci, S. Mao and J. Chen, *Adv Funct Mater*, 2015, **25**, 872-882.
8 K. J. Lee, S. J. Kim, J. J. Kim, K. Hwang, S. T. Kim and S. J. Park, *Opt Express*, 2014, **22 Suppl 4**, A1164-1173.
9 F. Yun, M. A. Reshchikov, L. He, H. Morkoc, C. K. Inoki and T. S. Kuan, *Appl Phys Lett*, 2002, **81**, 4142-4144.
10 C. Zhang, S. H. Park, D. Chen, D. W. Lin, W. Xiong, H. C. Kuo, C. F. Lin, H. Cao and J. Han, *ACS Photonics*, 2015, **2**, 980-986.
11 S. Jang, Y. Koh, J. Kim, J. Park, C. Park, S. J. Kim, S. Cho, Y. C. Ko and H. Sohn, *Materials Letters*, 2008, **62**, 552-555.
12 L. L. Zhang and X. S. Zhao, *Chem Soc Rev*, 2009, **38**, 2520-2531.
13 L. T. Canham, *Appl Phys Lett*, 1990, **57**, 1046.
14 A. G. Cullis, L. T. Canham and P. D. J. Calcott, *J Appl Phys*, 1997, **82**, 909.
15 W. J. Tseng, D. H. van Dorp, R. R. Lieten, P. M. Vereecken and G. Borghs, *J Phys Chem C*, 2014, **118**, 29492-29498.
16 J. Kim, S. S. Joo, K. W. Lee, J. H. Kim, D. H. Shin, S. Kim and S. H. Choi, *ACS applied materials & interfaces*, 2014, **6**, 20880-20886.
17 S. Zhuo, J. Zhang, Y. Shi, Y. Huang and B. Zhang, *Angewandte Chemie*, 2015, **54**, 5693-5696.
18 M. Zhang, Y. Wang, F. Teng, L. Chen, J. Li, J. Zhou, X. Pan and E. Xie, *Materials Letters*, 2016, **162**, 117-120.
19 G. Li, W. Wang, W. Yang, Y. Lin, H. Wang, Z. Lin and S. Zhou, *Reports on progress in physics. Physical Society*, 2016, **79**, 056501.
20 G. Li, W. Wang, W. Yang and H. Wang, *Surface Science Reports*, 2015, **70**, 380-423.
21 E. Munoz, E. Monroy, J. L. Pau, F. Calle, F. Omnes and P. Gibart, *J Phys-Condens Mat*, 2001, **13**, 7115-7137.
22 E. Monroy, F. Calle, E. Muñoz and F. Omnès, *Appl Phys Lett*, 1999, **74**, 3401.
23 W. Wang, H. Yang and G. Li, *Journal of Materials Chemistry C*, 2013, **1**, 4070.
24 J. C. Carrano, D. J. H. Lambert, C. J. Eiting, C. J. Collins, T. Li, S. Wang, B. Yang, A. L. Beck, R. D. Dupuis and J. C. Campbell, *Appl Phys Lett*, 2000, **76**, 924.
25 A. V. Sampath, Q. G. Zhou, R. W. Enck, D. McIntosh, H. Shen, J. C. Campbell and M. Wraback, *Appl Phys Lett*, 2012, **101**, 093506.
26 D. Li, X. Sun, H. Song, Z. Li, Y. Chen, H. Jiang and G. Miao, *Adv Mater*, 2012, **24**, 845-849.
27 G. Bao, D. Li, X. Sun, M. Jiang, Z. Li, H. Song, H. Jiang, Y. Chen, G. Miao and Z. Zhang, *Opt Express*, 2014, **22**, 24286-24293.
28 W. Zhang, J. Xu, W. Ye, Y. Li, Z. Qi, J. Dai, Z. Wu, C. Chen, J. Yin, J. Li, H. Jiang and Y. Fang, *Appl Phys Lett*, 2015, **106**, 021112.
29 S. H. Abud, Z. Hassan, F. K. Yam and C. W. Chin, *Measurement*, 2014, **50**, 172-174.

30 F. Peng, S. J. Qin, L. F. Hu, J. Y. Wang, J. M. Yang, X. Q. Chen and G. B. Pan, *Chem Phys Lett*, 2016, **652**, 6-10.
31 L. S. Chuah, Z. Hassan and H. Abu Hassan, *Optoelectron Adv Mat*, 2007, **1**, 400-403.
32 L. S. Chuah, Z. Hassan and H. Abu Hassan, *J Optoelectron Adv M*, 2007, **9**, 2886-2890.
33 W. J. Hsu, K. T. Chen, W. C. Huang, C. J. Wu, J. J. Dai, S. H. Chen and C. F. Lin, *Opt Express*, 2016, **24**, 11601-11610.
34 G. Yuan, K. Xiong, C. Zhang, Y. Li and J. Han, *ACS Photonics*, 2016, **3**, 1604-1610.
35 J. Yu, L. Zhang, J. Shen, Z. Xiu and S. Liu, *CrystEngComm*, 2016, **18**, 5149-5154.
36 P. C. Chang, C. L. Yu, S. J. Chang, Y. C. Lin, C. H. Liu and S. L. Wu, *Ieee Sens J*, 2007, **7**, 1270-1273.
37 K. Xu, C. Xu, Y. Y. Xie, J. Deng, Y. X. Zhu, W. L. Guo, M. Xun, K. B. K. Teo, H. D. Chen and J. Sun, *Ieee T Electron Dev*, 2015, **62**, 2802-2808.
38 J. L. Hou, S. J. Chang, M. C. Chen, C. H. Liu, T. J. Hsueh, J. K. Sheu and S. G. Li, *Ieee T Electron Dev*, 2013, **60**, 1178-1182.
39 C. Yang, L. Liu, S. C. Zhu, Z. G. Yu, X. Xi, S. T. Wu, H. C. Cao, J. M. Li and L. X. Zhao, *The Journal of Physical Chemistry C*, 2017, DOI: 10.1021/acs.jpcc.7b00748.
40 X. Gong, M. Tong, Y. Xia, W. Cai, J. S. Moon, Y. Cao, G. Yu, C. L. Shieh, B. Nilsson and A. J. Heeger, *Science*, 2009, **325**, 1665-1667.
41 L. Z. Hao, W. Gao, Y. J. Liu, Y. M. Liu, Z. D. Han, Q. Z. Xue and J. Zhu, *Physical chemistry chemical physics : PCCP*, 2016, **18**, 1131-1139.
42 F. Xie, H. Lu, X. Xiu, D. Chen, P. Han, R. Zhang and Y. Zheng, *Solid-State Electronics*, 2011, **57**, 39-42.
43 F. Xie, H. Lu, D. J. Chen, X. L. Ji, F. Yan, R. Zhang, Y. D. Zheng, L. Li and J. J. Zhou, *Ieee Sens J*, 2012, **12**.
44 J. S. Liu, C. X. Shan, B. H. Li, Z. Z. Zhang, C. L. Yang, D. Z. Shen and X. W. Fan, *Appl Phys Lett*, 2010, **97**, 251102.
45 E. Muñoz, E. Monroy, J. A. Garrido, I. Izpura, F. J. Sánchez, M. A. Sánchez-García, E. Calleja, B. Beaumont and P. Gibart, *Appl Phys Lett*, 1997, **71**, 870.
46 D. Li, X. Sun, H. Song, Z. Li, H. Jiang, Y. Chen, G. Miao and B. Shen, *Appl Phys Lett*, 2011, **99**, 261102.
47 R. Calarco, M. Marso, T. Richter, A. I. Aykanat, R. Meijers, V. D. H. A, T. Stoica and H. Luth, *Nano Lett*, 2005, **5**, 981-984.
48 K. H. Lee, P. C. Chang, S. J. Chang and S. L. Wu, *J Appl Phys*, 2011, **110**, 083113.
49 L. Sang, M. Liao, Y. Koide and M. Sumiya, *Appl Phys Lett*, 2011, **98**, 103502.
50 W. K. Hong, J. I. Sohn, D. K. Hwang, S. S. Kwon, G. Jo, S. Song, S. M. Kim, H. J. Ko, S. J. Park, M. E. Welland and T. Lee, *Nano Lett*, 2008, **8**, 950-956.
51 H. Kind, H. Q. Yan, B. Messer, M. Law and P. D. Yang, *Adv Mater*, 2002, **14**, 158-160.
52 Y. F. Cao, K. M. Cai, P. Hu, L. X. Zhao, T. Yan, W. G. Luo, X. Zhang, X. Wu, K. Y. Wang and H. Zheng, *Sci Rep*, 2015, **5**, 8130.
53 H. Y. Chen, K. W. Liu, X. Chen, Z. Z. Zhang, M. M. Fan, M. M. Jiang, X. H. Xie, H. F. Zhao and D. Z. Shen, *J. Mater. Chem. C*, 2014, **2**, 9689-9694.